iScience

CellPress
OPEN ACCESS

Article

Microneedle array delivery of *Yersinia pestis* recapitulates bubonic plague

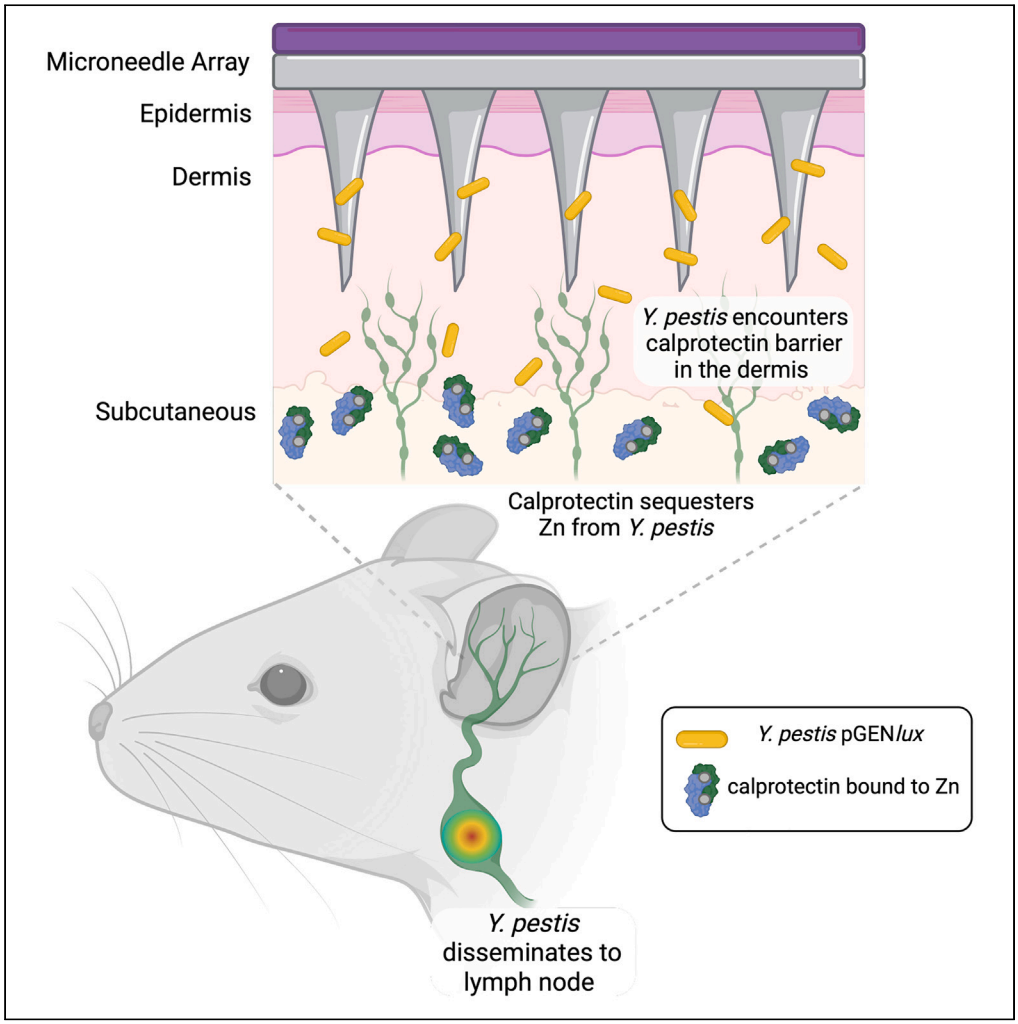

Sarah L. Price, Robert S. Oakes, Rodrigo J. Gonzalez, ..., Ulrich H. von Andrian, Christopher M. Jewell, Matthew B. Lawrenz

matt.lawrenz@louisville.edu

Highlights

MNAs reproducibly deliver *Y. pestis* to the dermis, mimicking flea transmission

MNA inoculation reveals *Y. pestis* encounters calprotectin in the dermis

Calprotectin Zn restriction inhibits dermal colonization and lymph node dissemination

MNA intradermal delivery of an attenuated *Y. pestis* suggests potential for vaccine

Price et al., iScience *27*, 108600
January 19, 2024
https://doi.org/10.1016/j.isci.2023.108600

iScience

CellPress
OPEN ACCESS

Article

Microneedle array delivery of *Yersinia pestis* recapitulates bubonic plague

Sarah L. Price,[1] Robert S. Oakes,[2,3] Rodrigo J. Gonzalez,[4,5] Camilla Edwards,[2] Amanda Brady,[1] Jennifer K. DeMarco,[1] Ulrich H. von Andrian,[4,5] Christopher M. Jewell,[2,3,6,7,8] and Matthew B. Lawrenz[1,9,10,*]

SUMMARY

Fleas transmit *Yersinia pestis* directly within the dermis of mammals to cause bubonic plague. Syringe-mediated inoculation is widely used to recapitulate bubonic plague and study *Y. pestis* pathogenesis. However, intradermal needle inoculation is tedious, error prone, and poses a significant safety risk for laboratorians. Microneedle arrays (MNAs) are micron-scale polymeric structures that deliver materials to the dermis, while minimizing the risk of needle sticks. We demonstrated that MNA inoculation is a viable strategy to recapitulate bubonic plague and study bacterial virulence by defining the parameters needed to establish a lethal infection in the mouse model and characterizing the course of infection using live-animal optical imaging. Using MNAs, we also demonstrated that *Y. pestis* must overcome calprotectin-mediated zinc restriction within the dermis and dermal delivery of an attenuated mutant has vaccine potential. Together, these data demonstrate that MNAs are a safe alternative to study *Y. pestis* pathogenesis in the laboratory.

INTRODUCTION

The gram-negative bacterium *Yersinia pestis* causes the disease bubonic plague, which is responsible for the most fatal pandemic in history known as the Black Death.[1–3] Currently, bubonic plague cases still occur in areas in which the bacterium is endemic in animal populations, including the southwestern United States.[4,5] Within these environments, *Y. pestis* is maintained within an enzootic cycle in which the bacterium is transmitted between mammalian hosts by a flea vector. During the feeding process, infected fleas deposit *Y. pestis* directly into the intradermal skin layer.[6,7] These bacteria then interact with host immune cells and rapidly disseminate from the skin to the draining lymph nodes.[8,9] Migration to the lymph nodes occurs minutes after infection and appears to be independent of intracellular trafficking by phagocytic cells.[8,9] Upon reaching the lymph nodes, *Y. pestis* evades clearance by resident immune cells and can replicate to high numbers. Eventually the bacteria breach the lymph node to disseminate into the bloodstream,[10] which is an important step in the transmission of *Y. pestis* to a new flea vector and continuing the enzootic cycle. Spillover into human populations occurs when individuals come into contact with these infected fleas.[11,12] Despite the persistence of *Y. pestis* in many countries and potential for human spillover infections, an FDA-approved vaccine is not available to prevent plague. A greater understanding of bacterial transmission and dissemination would significantly affect strategies for preventing and controlling the spread of *Y. pestis*.

In the past, subcutaneous injection of *Y. pestis* has been routinely used to model bubonic plague. While this approach has revealed many aspects of *Y. pestis* pathogenesis, growing evidence suggests that subcutaneous injection of *Y. pestis* does not completely recapitulate the disease kinetics of bubonic plague and lacks the ability to study important pathogen interactions at the initial site of infection in the dermis.[8,13] Therefore, investigators have started to employ intradermal injection models that have proven to be more biologically reminiscent of flea transmission.[10,13,14] Intradermal administration into the dermis of the ear has revealed that *Y. pestis* dissemination and kinetics of lethal infection are much quicker than rates observed from subcutaneous injection.[8,10] These studies highlight that, upon *Y. pestis* intradermal inoculation, a few bacteria travel rapidly to the draining lymph node, where they replicate to high numbers attracting an influx of immune cells that form a bubo.[8,10,15] At the site of inoculation within the dermis, *Y. pestis* encounters neutrophils, but the bacteria overcome the immune system to avoid clearance and eventually replicate at the infection site.[8,9,16] Neutrophils have important roles in nutritional immunity through the

[1]Department of Microbiology and Immunology, University of Louisville School of Medicine, Louisville, KY 40202, USA
[2]Fischell Department of Bioengineering, University of Maryland, College Park, MD 20742, USA
[3]Department of Veterans Affairs, VA Maryland Health Care System, Baltimore, MD 21201, USA
[4]Department of Immunology, Harvard Medical School, Boston, MA 02115, USA
[5]The Ragon Institute of MGH, MIT and Harvard, Cambridge, MA 02139, USA
[6]Robert E. Fischell Institute for Biomedical Devices, College Park, MD 20742, USA
[7]Department of Microbiology and Immunology, University of Maryland Medical School, Baltimore, MD 21201, USA
[8]Marlene and Stewart Greenebaum Cancer Center, University of Maryland Medical School, Baltimore, MD 21201, USA
[9]Center for Predictive Medicine for Biodefense and Emerging Infectious Diseases, University of Louisville, Louisville, KY 40202, USA
[10]Lead contact
*Correspondence: matt.lawrenz@louisville.edu
https://doi.org/10.1016/j.isci.2023.108600

release of proteins that restrict bacterial access to metals, including calprotectin that specifically sequesters zinc, manganese, and iron.[17–23] Using subcutaneous administration of *Y. pestis*, we have previously shown that calprotectin is the primary zinc acquisition barrier for *Y. pestis* during bubonic plague.[24] We also showed that the bacterium overcomes calprotectin metal restriction via the expression of two zinc acquisition systems, ZnuABC and yersiniabactin.[24] However, the tissue in which *Y. pestis* encounters calprotectin restriction during bubonic plague remains to be determined. Therefore, application of a model that more closely mimics natural flea transmission, such as intradermal inoculation, is key to understand where *Y. pestis* encounters nutritional immunity.

While intradermal injection has proven to be a valuable tool to study plague, it presents a difficult challenge within the Biosafety Level 3 (BSL-3) laboratory. The accurate application of a standard syringe needle to precisely inoculate the dermal layer of the skin while wearing appropriate personal protective equipment proves to be tedious and difficult. Moreover, these needles are significant safety hazards for laboratorians. Finally, common administration volumes needed to ensure reproducible inoculations (>20 μL) can cause tissue damage within the intradermal space that may stimulate an immune response unrelated to bacterial infection.[13] Therefore, a more efficient and safer technique to perform biologically relevant intradermal infections would significantly impact the adoption of the intradermal model for plague researchers. A unique option is presented by microneedle arrays (MNAs), which are micron-scale needles fabricated from biomaterials for drug and biologic delivery to defined intradermal depths.[25] Importantly, because of the micron length of the MNAs, they cannot puncture latex or nitrile gloves under normal application during research, significantly reducing the risk of self-inoculation encountered with standard syringe needles.[26] MNAs have been used extensively for vaccine and drug delivery and, more recently, have been adapted to specifically administer bacteria to the intradermal space.[25,27–29] For drug delivery, MNAs have been utilized to study mechanisms to combat methicillin-resistant *Staphylococcus aureus* (MRSA) and distribute antibiotic vancomycin directly to the infected skin area.[30] MNAs have been also used for a variety of vaccine studies, including immunizing with influenza antigen and with stabilized dengue virus.[28,31,32] Outside of studying infectious diseases, delivery by MNAs has shown an improvement for distribution of cancer vaccines and immunotherapies.[25] Finally, MNAs have been adapted to mimic intradermal tick transmission inoculation of *Francisella tularensis*.[29] The successful and reproducible intradermal delivery achieved in these studies suggests that MNAs may provide a useful tool to mimic flea transmission for the study of bubonic plague pathogenesis in the BSL-3 laboratory.

Here we show that MNA administration of *Y. pestis* reproducibly establishes intradermal instillation of *Y. pestis* that leads to lethal bubonic plague with disease kinetics previously reported for intradermal needle and flea inoculation. Furthermore, we demonstrate the utility of MNA administration as a tool to study *Y. pestis* virulence by using this model to establish that host calprotectin effectively limits *Y. pestis* zinc acquisition within the dermis. Finally, using an attenuated strain of *Y. pestis*, we show that MNA administration within the dermis has potential as a vaccine delivery platform against pulmonary infection.

RESULTS

MNAs reproducibly deliver *Y. pestis* to the dermis

Previous studies indicate that an infectious dose >200 colony-forming units (CFUs) of *Y. pestis* delivered via syringe inoculation to the ear pinna results in a reproducible lethal infection.[13,33] As such, our first step in adapting MNAs for *Y. pestis* inoculation was to establish conditions required to achieve reproducible inoculums within this range. The MNAs designed for this study were 650 μm from the MNA base to the tip to achieve penetration of the dermal layer.[34,35] Unlike syringes, solid, non-degradable MNAs do not actively inject materials into the dermal layer. Instead, these MNAs are coated with the transported substances or microorganisms and pressed onto the skin for delivery into the puncture sites.[29] Therefore, MNAs were incubated for 30 min with increasing bacterial concentrations (from 3×10^3 to 3×10^8 CFU/mL) to determine if an inoculum of 200–700 CFU could be achieved. After incubation, the MNA was placed on the bolus of the ear (Figure 1A), applied for 5 s, and then removed. 15 min later, ears were harvested, 70% ethanol was applied with a sterile swab to remove external bacteria, and subsets of ears were either fixed in 10% formalin and imaged by two-photon microscopy or homogenized using a tissue tearer and plated on selective agar to enumerate CFU (the limit of detection was 100 CFUs/tissue). Imaging of the ears revealed uniform needle inoculations across the dermal layer (Figure 1B) that appeared to travel approximately 30 μm into the tissue (Figure 1C and Video S1). We were unable to recover any bacteria from ears inoculated with MNAs incubated with inoculums below 3×10^5 CFU/mL (Figure 1D), indicating that less than 100 bacteria were administrated by MNAs incubated at these concentrations. However, bacteria were recovered from tissues inoculated with MNAs incubated with 3×10^6 CFU/mL and the number of CFU recovered increased as the inoculum increased to 3×10^8 CFU/mL (Figure 1D). Furthermore, we could detect rod-shaped bacteria at the inoculation site within the dermis layer (Figure 1E and Video S2). These data suggested that MNAs incubated with 3×10^7 CFU/mL delivered a dose within our desired range of ~500 CFU. To determine if these conditions yielded consistent reproducible inoculums, 15 mouse ears were inoculated with MNAs incubated with 3×10^7 CFU/mL and inoculums were calculated 15 min later. Bacterial enumeration showed a mean of 624 ± 129 CFUs recovered from the tissue (Figure 1F). Together, these data indicate that MNAs can consistently deliver *Y. pestis* into the dermis.

MNA inoculation results in a lethal *Y. pestis* infection that mimics that reported for flea inoculation

Intradermal inoculation via flea bite or needle injection results in deposition of *Y. pestis* into the dermis and rapid dissemination of a small population of bacteria to the draining lymph node.[8,9,16] Despite recruitment of resident neutrophils, the bacteria that remain in the dermis are able to survive and undergo limited proliferation.[8,13,36] To determine if MNA inoculation results in a similar disease manifestation, MNAs were used to inoculate mice with a *Y. pestis* strain expressing a bioluminescent bioreporter.[37] A subset of mice (n = 3) was euthanized at 15 min to confirm the inoculum (723 ± 384 CFUs), and optical imaging was used to monitor bacterial proliferation and dissemination as a function of

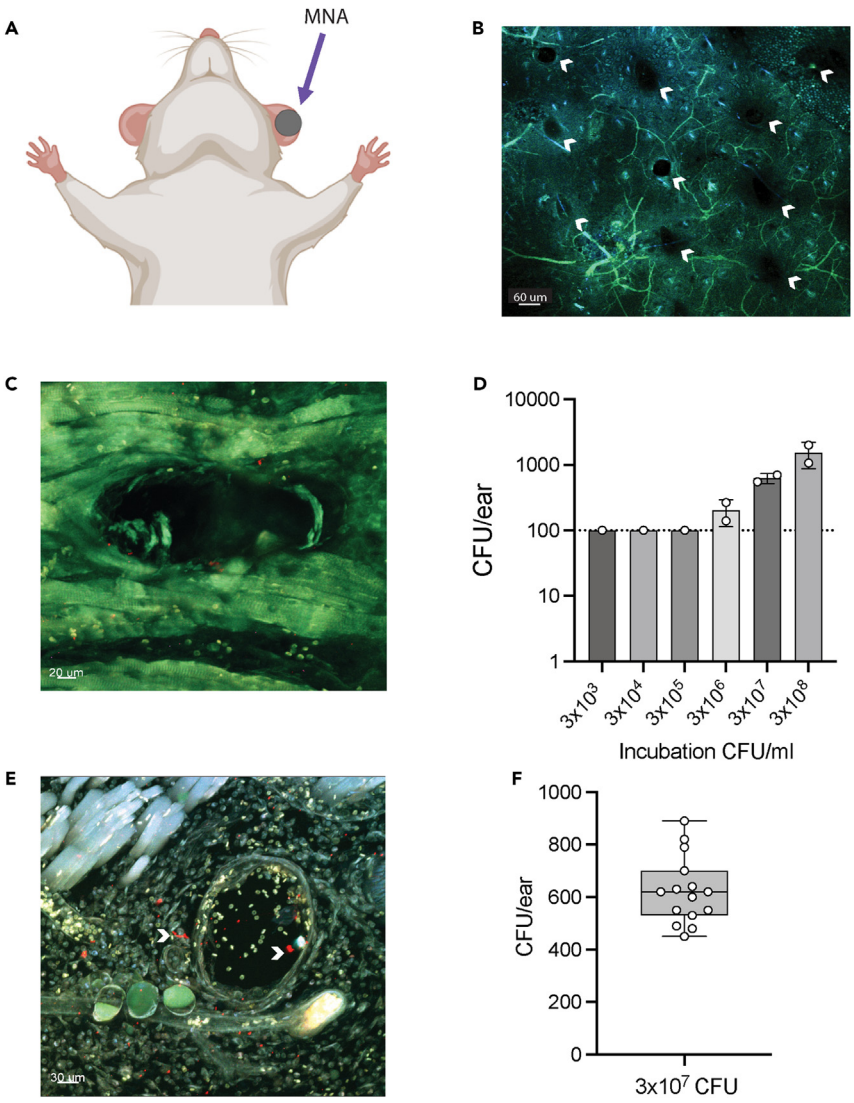

Figure 1. MNAs can reproducibly deliver *Y pestis* to the dermis

To determine the number of bacteria delivered by MNA infection, MNAs were incubated with increasing numbers of colony forming units (CFUs) of *Y. pestis* for 30 min.

(A) Mice are infected by applying the MNA to the left ear and applying pressure for 5 s. MNAs are removed with forceps after infection.

(B and C) Image of an ear inoculated with MNA without bacteria. White arrowheads denote MNA puncture sites.

(D) To determine the number of bacteria delivered to the dermis by MNAs, ears were harvested at 15 min post-infection with microarrays incubated with indicated concentrations of bacteria and recovered CFU were enumerated by serial dilution (mean ± S.D.). Dotted line indicates limit of detection.

(E) Image of MNA inoculation site from infected animal. White arrowheads denote bacteria (red).

(F) Bacterial CFU recovered from ears of mice infected with MNAs incubated with 3×10^7 CFU/mL. Each circle represents a single tissue (n = 15) harvested from two independent experiments.

bioluminescence in the remaining animals (Figures 2A–2C). At 0.25 h, bioluminescent bacteria were detected in the ears but not the cervical lymph nodes. By 12 h post-infection the signal in the ears decreased, most likely due to loss of bacteria that were originally deposited on the ear surface, but we observed bioluminescent signal in the cervical lymph nodes indicating lymph node colonization by this time point. Bioluminescence in both tissues increased over the remaining course of the infection, with the signal from both tissues peaking at 48 h post-inoculation (Figures 2A–2C). Conventional bacterial enumeration at 48 h post-inoculation confirmed robust colonization of both tissues by *Y. pestis* (Figure 2D). Furthermore, by 48 h post-inoculation, bioluminescent signal was detected in other tissues, indicating bacterial dissemination into the bloodstream (Figure 2C). Animals began to succumb to the infection by 60 h post-inoculation, with all animals meeting endpoint criteria by 72 h post-inoculation (Figure 2E). The kinetics of the infection using MNAs for inoculation closely recapitulates what

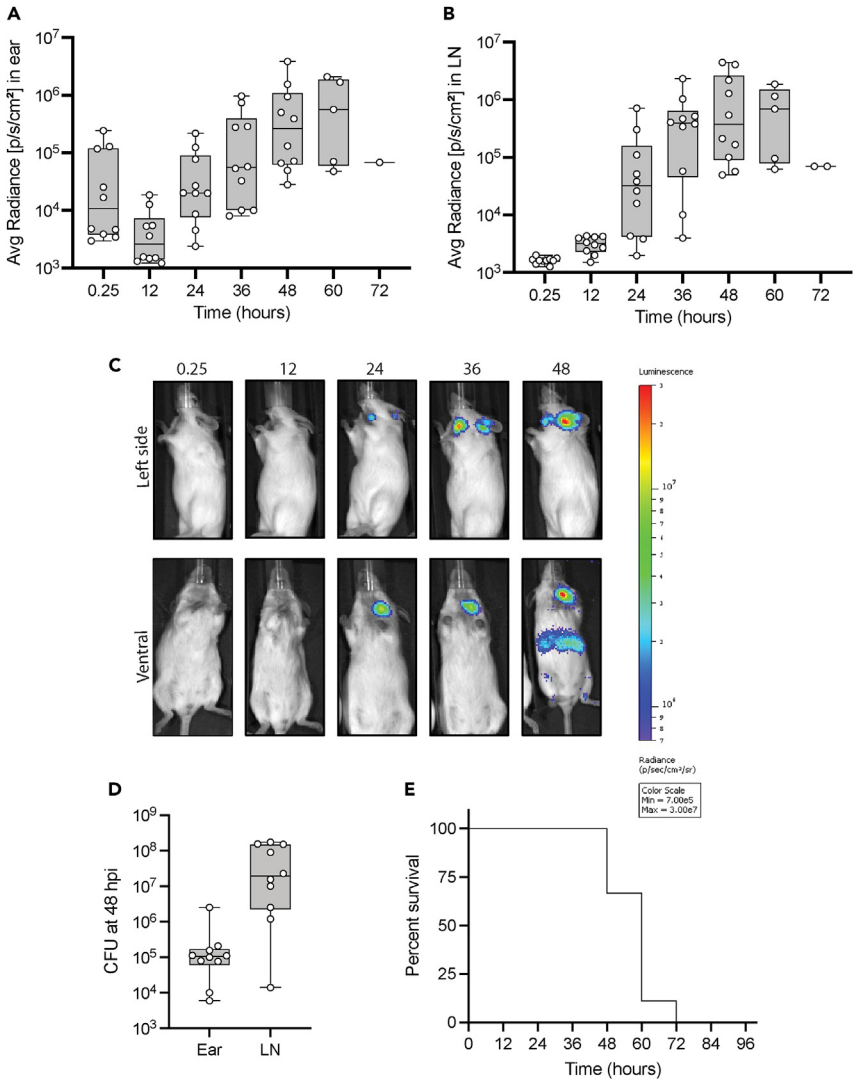

Figure 2. MNA inoculation results in a lethal *Y pestis* infection that mimics flea inoculation

To determine if *Y. pestis* infection follows similar kinetics of dissemination as a needle inoculation, Swiss Webster mice were infected intradermally with a bioluminescent strain of *Y. pestis* (combined data from two independent experiments; n = 5 per experiment). Bacterial dissemination and replication as a function of bioluminescence by optical imaging of the (A) ear and (B) draining LN.

(C) Representative mouse during optical imaging.

(D) Measurement of bacterial CFU in the ear and LN at 48 hpi.

(E) Survival curve of infected mice. Each point represents an individual mouse.

has been reported for intradermal needle inoculation or flea transmission,[8,36] supporting that MNA inoculation is a viable mechanism to model intradermal infections by *Y. pestis*.

MNA administration reveals the importance of calprotectin in restricting *Y. pestis* in the dermis

Using a subcutaneous injection model, we previously showed that calprotectin is the primary zinc sequestration barrier that *Y. pestis* needs to overcome to cause a lethal infection in mice.[24] While these studies showed that calprotectin protects mice from lethal infection by *Y. pestis* zinc acquisition mutants, the study design did not inform in which tissues *Y. pestis* encounters calprotectin-mediated zinc restriction during bubonic plague. Because neutrophils are a primary source of calprotectin[38] and rapidly recruited to the dermis during flea transmission of *Y. pestis*,[36] we next investigated if calprotectin restricts zinc availability for *Y. pestis* in the dermis. To test this hypothesis, C57Bl6/J and S100A9$^{-/-}$ (deficient in calprotectin) mice were inoculated using the MNAs with *Y. pestis* or a *Y. pestis* zinc acquisition mutant (*Y. pestis znuA ybtX)* expressing a bioluminescent bioreporter.[37] A subset of mice was euthanized at 15 min post-inoculation to confirm that equivalent

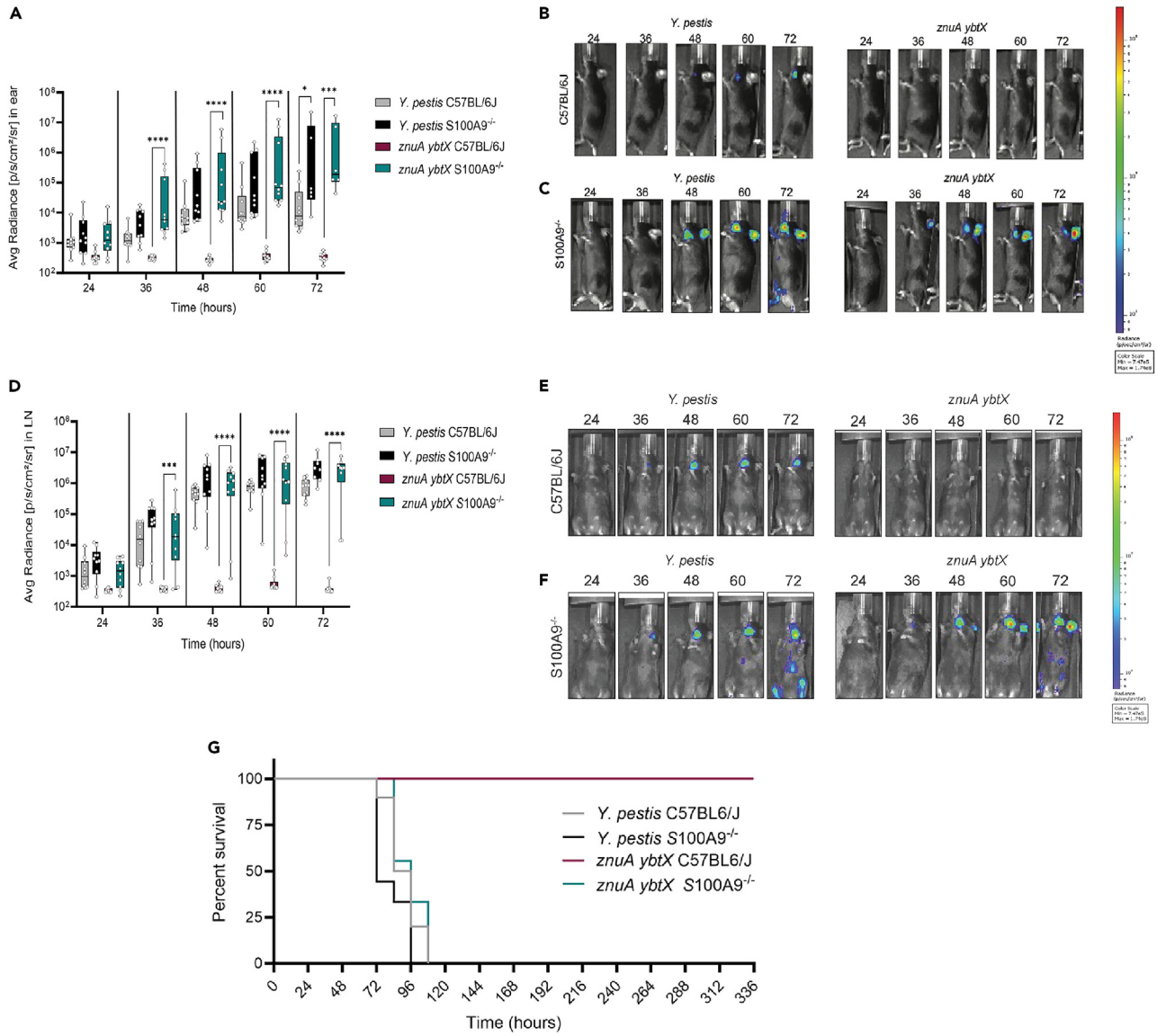

Figure 3. MNA administration reveals the importance of calprotectin in restricting *Y pestis* in the dermis

To determine tissues that *Y. pestis* encounters calprotectin, C57BL6/J or calprotectin-deficient (S100A9$^{-/-}$) mice (n = 10) were infected intradermally with bioluminescent strains of *Y. pestis* or a *znuA ybtX* mutant.

(A) Bacterial dissemination and replication as a function of bioluminescence measured by optical imaging in infected ears. Representative ear imaging for (B) C57BL6/J or (C) S100A9$^{-/-}$ mice.

(D) Bacterial dissemination and replication as a function of bioluminescence measured by optical imaging in the draining LN. Representative LN imaging for (E) C57BL6/J and (F) S100A9$^{-/-}$ mice.

(G) Survival curve of infected mice. For optical imaging: Two-tailed t test; * = $p < 0.05$, *** = $p < 0.001$, **** = $p < 0.0001$. For survival curves: Log rank test; C57BL6/J *Y. pestis* vs. C57BL6/J *znuA ybtX* - $p < 0.001$; C57BL6/J *znuA ybtX* vs. S100A9$^{-/-}$ *znuA ybtX* - $p < 0.001$.

inoculums were delivered (750 ± 117 and 526 ± 183, respectively), and bacterial proliferation and dissemination were monitored in the remaining mice by optical imaging. Greater bioluminescence was detected at each time point in the ears of S100A9$^{-/-}$ mice compared to C57BL6/J mice infected with *Y. pestis* (Figures 3A and 3B), suggesting that calprotectin restricts bacterial proliferation within the dermis. Calprotectin restriction was further supported by infection with the *znuA ybtX* mutant, which was unable to replicate in the dermis of C57Bl/6J mice but robustly replicated in the dermis of S100A9$^{-/-}$ mice (Figures 3A and 3B). *Y. pestis* also appeared to more rapidly disseminate to the draining lymph node and/or was better able to proliferate within these tissues in S100A9$^{-/-}$ mice than C57Bl/6J mice (Figures 3C and 3D). Moreover, S100A9$^{-/-}$ mice succumbed to infection with *Y. pestis* quicker than C57Bl/6J mice (mean time to death of 72 h vs. 90 h, respectively; $p = 0.109$) (Figure 3E). As we reported previously using the subcutaneous injection model,[24] S100A9$^{-/-}$ mice were unable to survive challenge

by the *znuA ybtX* zinc acquisition mutant, while C57Bl/6 mice survived (Figure 3E; $p < 0.0001$). Together, instillation by MNAs allowed us to demonstrate that calprotectin is an obstacle to *Y. pestis* infection within the dermis and a potent barrier for bacterial zinc acquisition within this tissue.

MNA delivery of attenuated *Y. pestis* changes disease kinetics in subsequent challenge

MNA delivery of vaccine candidates to the dermis can induce robust immune responses that protect against pulmonary challenge with influenza A virus and *F. novicida*.[29,31] Because the *znuA ybtX* mutant is severely attenuated for bubonic plague, we next investigated if the mice that survived MNA administration with the *znuA ybtX* mutant might be protected from subsequent pulmonary infection with *Y. pestis*. Therefore, C57Bl/6J mice were inoculated with *Y. pestis* or *Y. pestis znuA ybtX* and monitored for the development of moribund disease for 14 days. As expected, all mice challenged with *Y. pestis* succumbed to infection while those challenged with the *znuA ybtX* mutant survived the infection (Figure 4A). Optical imaging showed a similar pattern of proliferation and dissemination in the ears and draining lymph nodes as observed in Figure 3 (Figures 4B and 4C), and, importantly, no bioluminescence signal above background was detected in the tissues of *znuA ybtX* infected mice (Figures 4B and 4C). On day 14, the mice that survived MNA inoculation with *znuA ybtX* and a naive group of mice were infected with bioluminescent *Y. pestis* by intranasal administration and monitored for the development of lethal infection. Optical imaging of the thoracic cavity indicated slower proliferation of *Y. pestis* in the lungs of animals that were previously exposed to the *znuA ybtX* mutant, but ultimately the mice were not able to inhibit bacterial proliferation (Figures 4D and 4E). However, slower proliferation in the *znuA ybtX*-exposed mice directly correlated with a significant delay in lethality compared to naive infected mice (Figure 4E; mean time to death of 96 h vs. 60 h, respectively; $p = 0.0002$). Together, these data indicate that despite the inability of the *znuA ybtX* mutant to proliferate and disseminate, mice were mounting a systemic immune response to the bacteria, though a longer time or repeated MNA administration may be required to generate a fully protective response.

DISCUSSION

While subcutaneous inoculation has been a valuable tool to study bubonic plague pathogenesis, intradermal inoculation is more biologically relevant to natural flea transmission of *Y. pestis*.[39] Previously, MNAs have been used for mouse infections with *F. novicida*,[29] another bacterium transmitted by an arthropod vector. Building on these studies, we developed and characterized a similar model for *Y. pestis* inoculation in the ear pinna using MNAs, which is a safer and more efficient tool than typical needle inoculation.[27] Our first goal was to ensure that infection with MNAs would provide dissemination kinetics similar to those reported in studies of flea or other intradermal infection models with *Y. pestis*.[8–10] These previous studies suggest that, upon infection in the dermal layer, a few bacteria immediately travel via lymphatic vessels to the draining lymph node and begin to replicate to establish infection.[8–10] In a direct comparison between intradermal and subcutaneous routes of infection, Gonzalez et al. demonstrated that lymph node colonization occurred more rapidly with the intradermal infection route.[13] Using bioluminescent imaging, we recapitulated these results and observed lymph node colonization within 12 h of inoculation, with the peak bioluminescence observed at 48 h post-inoculation. Importantly, these data are also similar to infection with *Y. pestis* by flea inoculation.[9] Furthermore, our MNA infection model shows a rapid progression to lethality, which correlates with previous needle intradermal infections for plague pathogenesis.[13] It has been speculated that lethality in the intradermal bubonic model is faster than subcutaneous injection because of greater presence of, or access to, lymphatic vessels in the dermal layer of the skin.[13] It is also important to note that the volume administered by needle injection can influence the host response, with larger volumes (>2 μL) causing tissue damage and potential administration beyond the intradermal space.[13,40,41] Not only does a smaller inoculation more closely match a flea bite and cause less tissue damage but it also is less favorable for the bacteria.[13] Importantly because the microneedles do not deposit large volumes into the tissue, the bacteria are delivered directly within the intradermal space without similar concerns of mislocalization of bacteria due to changes in inoculum volumes.[27] Overall, these data support that the MNA infection model is biologically applicable to bubonic plague infection that is administered through a flea bite.

Using MNAs, we recapitulated previous findings that calprotectin is the main obstacle for zinc acquisition during *Y. pestis* infection (Figure 3).[24] However, by combining MNA administration with optical imaging of bacterial mutants, we were able to expand on these initial studies and show that *Y. pestis* encounters calprotectin-mediated zinc sequestration within the dermis during bubonic plague. These data indicate that *Y. pestis* needs to rapidly adjust to metal limitation upon flea transmission and that zinc acquisition is essential for the bacterium to colonize the dermis. Moreover, these data also demonstrate that we can use *Y. pestis* MNA administration to better define host-pathogen interactions specifically within the dermis, which has different cell types and immune responses than other tissues. For example, while neutrophils have been implicated as the primary source for calprotectin during immune responses in the lungs and liver,[42–44] a study using skin biopsies of Lyme disease patients suggests that other cell types are the primary source for calprotectin-mediated metal limitation in the dermis.[45] With the establishment of this reproducible dermal model of infection, moving forward we can use *Y. pestis* as a tool to better understand the mechanisms involved in nutritional immunity within the dermis.

With plague cases still occurring worldwide, there remains a need for a vaccine. Due to differences in lymphatic vascularization between the dermal layer and subcutaneous level in the skin,[46] intradermal and subcutaneous inoculations show differences in immune responses, with intradermal vaccines generating a more robust mucosal immune response.[13,47–49] Recent successes with MNA-delivered vaccines suggest an MNA platform can provide a strong mucosal immune response.[29,31] While vaccination was not the primary goal of these studies, we were able to show that intradermal delivery of an attenuated *Y. pestis* strain had an impact on subsequent pulmonary challenge—slower replication and a delay in the development of lethal infection. While a change in overall survival was not observed, likely because of the limited

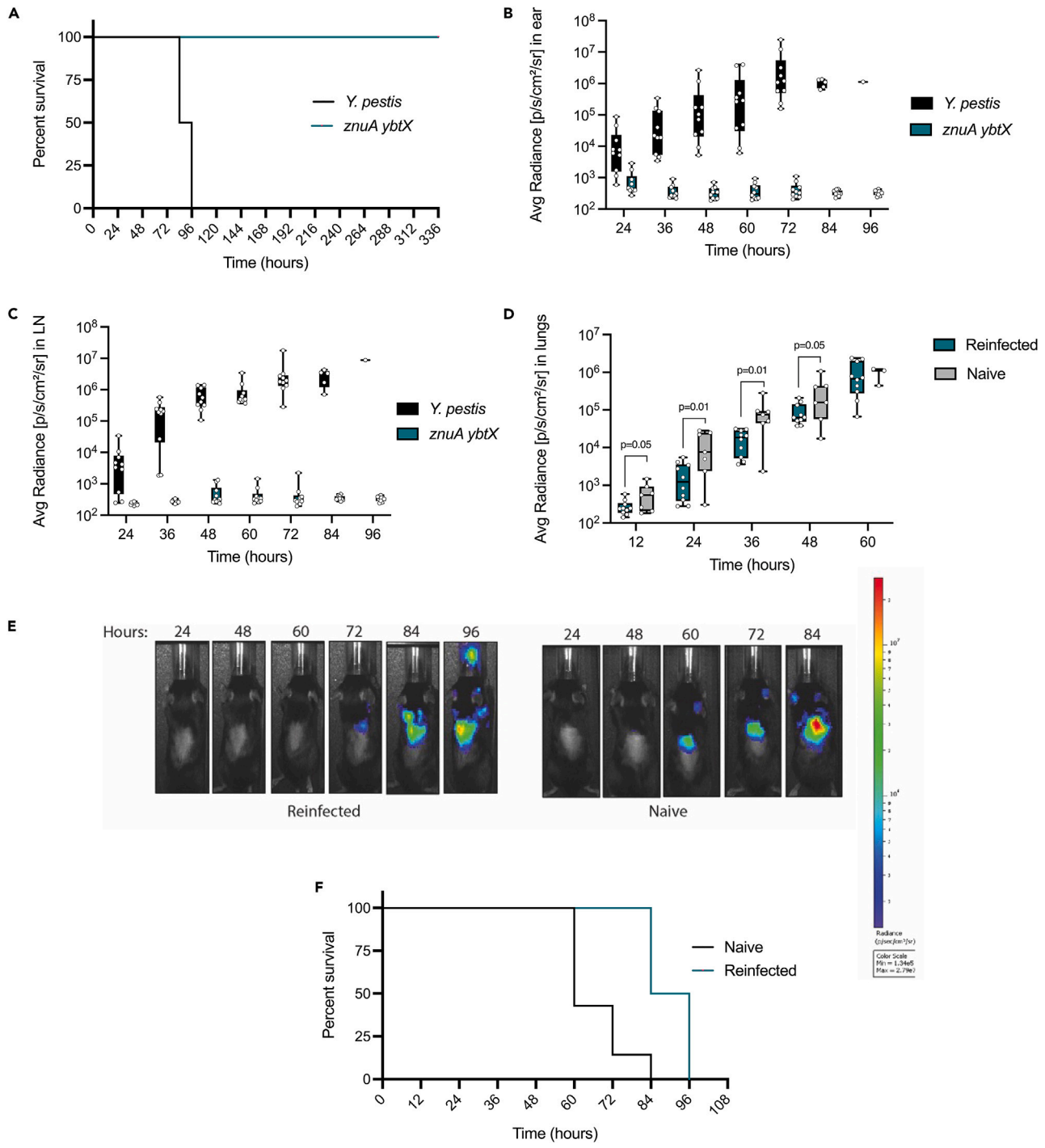

Figure 4. MNA delivery of attenuated *Y pestis* changes disease kinetics in subsequent challenge

To determine the potential for using MNA infection with the *znuA ybtX* mutant as a vaccine platform, (A) C57Bl/6J mice (n = 10) were infected via MNAs with *Y. pestis* and *znuA ybtX* (inoculum = 1 × 10^2) and monitored for 14 days.

(B and C) Bacterial dissemination and replication as a function of bioluminescence measured by optical imaging in infected ears and draining LNs.

(D) Bacterial replication as a function of bioluminescence measured by optical imaging in the thoracic cavity after *Y. pestis* intranasal inoculation of mice that survived *znuA ybtX* infection.

(E) Representative mice during optical imaging after reinoculation with *Y. pestis*.

(F) Survival curve of infected mice. For optical imaging: two-tailed t test. For survival curves: log rank test: p = 0.002.

time frame that mice were allowed to recover from challenge and generate a robust immune response, these studies provide preliminary data that MNA delivery of a vaccine may result in effective protection against pneumonic plague and justify future studies specifically designed for vaccination (i.e., prime-boost scenarios, measurements of immune responses, different vaccine formulations, etc.).

Limitations of the study

In this study, we established a model to mimic flea inoculation of *Y. pestis* using MNAs and applied this model to demonstrate that calprotectin-mediated zinc limitation in the dermis is a barrier to *Y. pestis* infection. We also used the model to provide preliminary evidence that an attenuated strain of *Y. pestis* introduced into the dermis via MNA inoculation has the potential to generate protective immune responses against subsequent exposure to pneumonic plague. While MNA inoculation is a model for flea transmission, like other laboratory models, inoculation via MNAs will not be able to account for flea-derived factors that may contribute to transmission during natural flea inoculation. Moreover, while *Y. pestis* encounters calprotectin in the dermis, the cellular source of calprotectin remains unresolved. Finally, while these data indicate that a protective immune response is generated after exposure to the attenuated *Y. pestis* zinc acquisition mutant, more refined studies, including direct measurement of immune responses and optimized exposure times, are required to fully understand the adaptive immune response generated via this model and to identify correlates of protection.

STAR★METHODS

Detailed methods are provided in the online version of this paper and include the following:

- KEY RESOURCES TABLE
- RESOURCE AVAILABILITY
  - Lead contact
  - Materials availability
  - Data and code availability
- EXPERIMENTAL MODEL AND STUDY PARTICIPANT DETAILS
  - Animals
  - Bacterial strains
- METHOD DETAILS
  - Microneedle array preparation
  - MNA incubation with *Y. pestis*
  - Animal infections with *Y. pestis*
  - Measurement of bacterial burden in the ear and lymph node
- IMAGING OF EAR WITH TWO-PHOTON MICROSCOPY
- QUANTIFICATION AND STATISTICAL ANALYSIS

SUPPLEMENTAL INFORMATION

Supplemental information can be found online at https://doi.org/10.1016/j.isci.2023.108600.

ACKNOWLEDGMENTS

The authors would like to thank Drs. Thomas Vogl at the University of Muenster and Thomas Kehl-Fie at the University of Illinois Urbana-Champaign for sharing the S100A9$^{-/-}$ mice and Drs. Robert Ernst and Courtney Chandler at the University of Maryland for providing training for MNA inoculations. The authors also thank the University of Louisville's Center for Predictive Medicine for Biodefense and Emerging Infectious Diseases Shared Resources and Vivarium Staff for technical support during these studies. We acknowledge the support of the Maryland NanoCenter and its AIMLab for their help in obtaining SEM images. This work was supported by funding from the National Institutes of Health T32AI132146 (S.L.P.), F31AI147404 (S.L.P.), R01AI144667 (C.M.J.), R21AI135225 (M.B.L.), R01AI148241 (M.B.L.), P20GM125504 (M.B.L.), the United States Department of Veterans Affairs IK2BX005061 (R.S.O.), and in part by the Jewish Heritage Foundation for Excellence Grant Program at the University of Louisville School of Medicine (M.B.L.).

AUTHOR CONTRIBUTIONS

S.L.P. and M.B.L. conceived and designed all experiments. S.L.P. contributed to all experiments. R.S.O. and C.M.J. generated MNAs. R.J.G. performed imaging of ears with two-photon microscopy. C.E. performed SEM and DMA studies. A.B. and J.K.D. contributed to animal studies. S.L.P. and M.B.L. analyzed data. S.L.P. and M.B.L. wrote the manuscript with comments and revisions from R.S.O., R.J.G., J.K.D., A.B., and C.M.J.

DECLARATION OF INTERESTS

C.M.J. and R.S.O. are employees of the VA Maryland Healthcare System. The views in this paper do not reflect the views of the Department of Veterans Affairs or the United States Government. C.M.J. has equity positions in Cartesian Therapeutics and Vaccitech PLC.

Received: July 15, 2023
Revised: September 25, 2023
Accepted: November 28, 2023
Published: November 30, 2023

REFERENCES

1. Perry, R.D., and Fetherston, J.D. (1997). *Yersinia pestis* - etiologic agent of plague. Clin. Microbiol. Rev. *10*, 35–66.
2. Pollitzer, R. (1951). Plague studies. Bull. World Health Organ. *4*, 475–533.
3. Bos, K.I., Schuenemann, V.J., Golding, G.B., Burbano, H.A., Waglechner, N., Coombes, B.K., McPhee, J.B., DeWitte, S.N., Meyer, M., Schmedes, S., et al. (2011). A draft genome of *Yersinia pestis* from victims of the Black Death. Nature *478*, 506–510.
4. Stenseth, N.C., Atshabar, B.B., Begon, M., Belmain, S.R., Bertherat, E., Carniel, E., Gage, K.L., Leirs, H., and Rahalison, L. (2008). Plague: past, present, and future. PLoS Med. *5*, e3.
5. Butler, T. (2013). Plague Gives Surprises in the First Decade of the 21st Century in the United States and Worldwide. Am. J. Trop. Med. Hyg. *89*, 788–793.
6. Sebbane, F., Jarrett, C.O., Gardner, D., Long, D., and Hinnebusch, B.J. (2006). Role of the *Yersinia pestis* plasminogen activator in the incidence of distinct septicemic and bubonic forms of flea-borne plague. Proc. Natl. Acad. Sci. USA *103*, 5526–5530.
7. Hinnebusch, B.J. (2005). The Evolution of Flea-Borne Transmission in *Yersinia pestis*. Curr. Issues Mol. Biol. *7*, 197–212.
8. Gonzalez, R.J., Lane, M.C., Wagner, N.J., Weening, E.H., and Miller, V.L. (2015). Dissemination of a highly virulent pathogen: tracking the early events that define infection. PLoS Pathog. *11*, e1004587.
9. Shannon, J.G., Hasenkrug, A.M., Dorward, D.W., Nair, V., Carmody, A.B., and Hinnebusch, B.J. (2013). *Yersinia pestis* Subverts the Dermal Neutrophil Response in a Mouse Model of Bubonic Plague. mBio *4*, e00170-13.
10. Sebbane, F., Gardner, D., Long, D., Gowen, B.B., and Hinnebusch, B.J. (2005). Kinetics of Disease Progression and Host Response in a Rat Model of Bubonic Plague. Am. J. Pathol. *166*, 1427–1439.
11. Bacot, A.W., and Martin, C.J. (1914). LXVII. Observations on the mechanism of the transmission of plague by fleas. J. Hyg. *13*, 423–439.
12. Bacot, A.W. (1915). LXXXI. Further notes on the mechanism of the transmission of plague by fleas. J. Hyg. *14*, 774–776.3.
13. Gonzalez, R.J., Weening, E.H., Lane, M.C., and Miller, V.L. (2015). Comparison of Models for Bubonic Plague Reveals Unique Pathogen Adaptations to the Dermis. Infect. Immun. *83*, 2855–2861.
14. Hinnebusch, B.J. (2004). Interactions of *Yersinia pestis* with its flea vector that lead to the transmission of plague. In *Microbe-Vector Interactions in Vector-Borne Diseases*. Society for General Microbiology Symposia, S.H. Gillespie, G.L. Smith, and A. Osbourn, eds. (Cambridge: Cambridge University Press), pp. 331–344.
15. Guinet, F., Avé, P., Jones, L., Huerre, M., and Carniel, E. (2008). Defective Innate Cell Response and Lymph Node Infiltration Specify *Yersinia pestis* Infection. PLoS One *3*, e1688.
16. Gonzalez, R.J., Lane, M.C., Wagner, N.J., Weening, E.H., and Miller, V.L. (2015). Dissemination of a Highly Virulent Pathogen: Tracking The Early Events That Define Infection. PLoS Pathog. *11*, e1004587.
17. Gaddy, J.A., Radin, J.N., Loh, J.T., Piazuelo, M.B., Kehl-Fie, T.E., Delgado, A.G., Ilca, F.T., Peek, R.M., Cover, T.L., Chazin, W.J., et al. (2014). The host protein calprotectin modulates the *Helicobacter pylori* cag type IV secretion system via zinc sequestration. PLoS Pathog. *10*, e1004450.
18. Hood, M.I., Mortensen, B.L., Moore, J.L., Zhang, Y., Kehl-Fie, T.E., Sugitani, N., Chazin, W.J., Caprioli, R.M., and Skaar, E.P. (2012). Identification of an *Acinetobacter baumannii* zinc acquisition system that facilitates resistance to calprotectin-mediated zinc sequestration. PLoS Pathog. *8*, e1003068.
19. Kehl-Fie, T.E., Zhang, Y., Moore, J.L., Farrand, A.J., Hood, M.I., Rathi, S., Chazin, W.J., Caprioli, R.M., and Skaar, E.P. (2013). MntABC and MntH Contribute to Systemic *Staphylococcus aureus* Infection by Competing with Calprotectin for Nutrient Manganese. Infect. Immun. *81*, 3395–3405.
20. Urban, C.F., Ermert, D., Schmid, M., Abu-Abed, U., Goosmann, C., Nacken, W., Brinkmann, V., Jungblut, P.R., and Zychlinsky, A. (2009). Neutrophil extracellular traps contain calprotectin, a cytosolic protein complex involved in host defense against *Candida albicans*. PLoS Pathog. *5*, e1000639.
21. Besold, A.N., Gilston, B.A., Radin, J.N., Ramsoomair, C., Culbertson, E.M., Li, C.X., Cormack, B.P., Chazin, W.J., Kehl-Fie, T.E., and Culotta, V.C. (2018). Role of Calprotectin in Withholding Zinc and Copper from *Candida albicans*. Infect. Immun. *86*, e00779-17.
22. Ammendola, S., Secli, V., Pacello, F., Mastropasqua, M.C., Romão, M.A., Gomes, C.M., and Battistoni, A. (2022). Zinc-binding metallophores protect *Pseudomonas aeruginosa* from calprotectin-mediated metal starvation. FEMS Microbiol. Lett. *369*, fnac071.
23. Liu, J.Z., Jellbauer, S., Poe, A.J., Ton, V., Pesciaroli, M., Kehl-Fie, T.E., Restrepo, N.A., Hosking, M.P., Edwards, R.A., Battistoni, A., et al. (2012). Zinc sequestration by the neutrophil protein calprotectin enhances *Salmonella* growth in the inflamed gut. Cell Host Microbe *11*, 227–239.
24. Price, S.L., Vadyvaloo, V., DeMarco, J.K., Brady, A., Gray, P.A., Kehl-Fie, T.E., Garneau-Tsodikova, S., Perry, R.D., and Lawrenz, M.B. (2021). Yersiniabactin contributes to overcoming zinc restriction during *Yersinia pestis* infection of mammalian and insect hosts. Proc. Natl. Acad. Sci. USA *118*, e2104073118.
25. Zeng, Q., Gammon, J.M., Tostanoski, L.H., Chiu, Y.-C., and Jewell, C.M. (2017). In Vivo Expansion of Melanoma-Specific T Cells Using Microneedle Arrays Coated with Immune-Polyelectrolyte Multilayers. ACS Biomater. Sci. Eng. *3*, 195–205.
26. Martin, A., McConville, A., Anderson, A., McLister, A., and Davis, J. (2017). Microneedle Manufacture: Assessing Hazards and Control Measures. Saf. Now. *3*, 25.
27. Donnelly, R.F., Singh, T.R.R., Tunney, M.M., Morrow, D.I.J., McCarron, P.A., O'Mahony, C., and Woolfson, A.D. (2009). Microneedle arrays allow lower microbial penetration than hypodermic needles in vitro. Pharm. Res. (N. Y.) *26*, 2513–2522.
28. Rouphael, N.G., Paine, M., Mosley, R., Henry, S., McAllister, D.V., Kalluri, H., Pewin, W., Frew, P.M., Yu, T., Thornburg, N.J., et al. (2017). The safety, immunogenicity, and acceptability of inactivated influenza vaccine delivered by microneedle patch (TIV-MNP 2015): a randomised, partly blinded, placebo-controlled, phase 1 trial. Lancet Lond. Engl. *390*, 649–658.
29. Chandler, C.E., Harberts, E.M., Laemmermann, T., Zeng, Q., Opene, B.N., Germain, R.N., Jewell, C.M., Scott, A.J., and Ernst, R.K. (2018). *In Vivo* Intradermal Delivery of Bacteria by Using Microneedle Arrays. Infect. Immun. *86*, e00406-18.
30. Ziesmer, J., Tajpara, P., Hempel, N.-J., Ehrström, M., Melican, K., Eidsmo, L., and Sotiriou, G.A. (2021). Vancomycin-Loaded Microneedle Arrays against Methicillin-Resistant *Staphylococcus aureus* Skin Infections. Adv. Mater. Technol. *6*, 2001307.
31. Zhu, Q., Zarnitsyn, V.G., Ye, L., Wen, Z., Gao, Y., Pan, L., Skountzou, I., Gill, H.S., Prausnitz, M.R., Yang, C., and Compans, R.W. (2009). Immunization by vaccine-coated microneedle arrays protects against lethal influenza virus challenge. Proc. Natl. Acad. Sci. *106*, 7968–7973.
32. Turvey, M.E., Uppu, D.S.S.M., Mohamed Sharif, A.R., Bidet, K., Alonso, S., Ooi, E.E., and Hammond, P.T. (2019). Microneedle-based intradermal delivery of stabilized dengue virus. Bioeng. Transl. Med. *4*, e10127.
33. Gonzalez, R.J., Weening, E.H., Frothingham, R., Sempowski, G.D., and Miller, V.L. (2012). Bioluminescence imaging to track bacterial dissemination of *Yersinia pestis* using different routes of infection in mice. BMC Microbiol. *12*, 147.
34. Bookstaver, M.L., Tsai, S.J., Bromberg, J.S., and Jewell, C.M. (2018). Improving Vaccine and Immunotherapy Design Using Biomaterials. Trends Immunol. *39*, 135–150.
35. Makvandi, P., Kirkby, M., Hutton, A.R.J., Shabani, M., Yiu, C.K.Y., Baghbantaraghdari, Z., Jamaledin, R., Carlotti, M., Mazzolai, B., Mattoli, V., and Donnelly, R.F. (2021). Engineering Microneedle Patches for Improved Penetration: Analysis, Skin Models and Factors Affecting Needle Insertion. Nano-Micro Lett. *13*, 93.
36. Shannon, J.G., Bosio, C.F., and Hinnebusch, B.J. (2015). Dermal Neutrophil, Macrophage and Dendritic Cell Responses to *Yersinia pestis* Transmitted by Fleas. PLoS Pathog. *11*, e1004734.

37. Sun, Y., Connor, M.G., Pennington, J.M., and Lawrenz, M.B. (2012). Development of bioluminescent bioreporters for *in vitro* and *in vivo* tracking of *Yersinia pestis*. PLoS One *7*, e47123.
38. Dale, I., Fagerhol, M.K., and Naesgaard, I. (1983). Purification and Partial Characterization of a Highly Immunogenic Human Leukocyte Protein, the L1 Antigen. Eur. J. Biochem. *134*, 1–6.
39. Chong, S.Z., Evrard, M., and Ng, L.G. (2013). Lights, Camera, and Action: Vertebrate Skin Sets the Stage for Immune Cell Interaction with Arthropod-Vectored Pathogens. Front. Immunol. *4*, 286.
40. Guinet, F., and Carniel, E. (2003). A technique of intradermal injection of *Yersinia* to study *Y. pestis* physiopathology. Adv. Exp. Med. Biol. *529*, 73–78.
41. Bosio, C.F., Jarrett, C.O., Gardner, D., and Hinnebusch, B.J. (2012). Kinetics of innate immune response to *Yersinia pestis* after intradermal infection in a mouse model. Infect. Immun. *80*, 4034–4045.
42. Damo, S.M., Kehl-Fie, T.E., Sugitani, N., Holt, M.E., Rathi, S., Murphy, W.J., Zhang, Y., Betz, C., Hench, L., Fritz, G., et al. (2013). Molecular basis for manganese sequestration by calprotectin and roles in the innate immune response to invading bacterial pathogens. Proc Natl Acad Sci USA *110*, 3841–3846.
43. Kehl-Fie, T.E., Chitayat, S., Hood, M.I., Damo, S., Restrepo, N., Garcia, C., Munro, K.A., Chazin, W.J., and Skaar, E.P. (2011). Nutrient metal sequestration by calprotectin inhibits bacterial superoxide defense, enhancing neutrophil killing of *Staphylococcus aureus*. Cell Host Microbe *10*, 158–164.
44. Clark, H.L., Jhingran, A., Sun, Y., Vareechon, C., de Jesus Carrion, S., Skaar, E.P., Chazin, W.J., Calera, J.A., Hohl, T.M., and Pearlman, E. (2016). Zinc and Manganese Chelation by Neutrophil S100A8/A9 (Calprotectin) Limits Extracellular *Aspergillus fumigatus* Hyphal Growth and Corneal Infection. J. Immunol. *196*, 336–344.
45. Besold, A.N., Culbertson, E.M., Nam, L., Hobbs, R.P., Boyko, A., Maxwell, C.N., Chazin, W.J., Marques, A.R., and Culotta, V.C. (2018). Antimicrobial action of calprotectin that does not involve metal withholding. Metallomics *10*, 1728–1742.
46. O'Mahony, S., Rose, S.L., Chilvers, A.J., Ballinger, J.R., Solanki, C.K., Barber, R.W., Mortimer, P.S., Purushotham, A.D., and Peters, A.M. (2004). Finding an optimal method for imaging lymphatic vessels of the upper limb. Eur. J. Nucl. Med. Mol. Imaging *31*, 555–563.
47. Cubas, R., Zhang, S., Kwon, S., Sevick-Muraca, E.M., Li, M., Chen, C., and Yao, Q. (2009). Virus-like particle (VLP) Lymphatic Trafficking and Immune Response Generation after Immunization by Different Routes. J. Immunother. *32*, 118–128.
48. Liard, C., Munier, S., Arias, M., Joulin-Giet, A., Bonduelle, O., Duffy, D., Shattock, R.J., Verrier, B., and Combadière, B. (2011). Targeting of HIV-p24 particle-based vaccine into differential skin layers induces distinct arms of the immune responses. Vaccine *29*, 6379–6391.
49. Bonnotte, B., Gough, M., Phan, V., Ahmed, A., Chong, H., Martin, F., and Vile, R.G. (2003). Intradermal injection, as opposed to subcutaneous injection, enhances immunogenicity and suppresses tumorigenicity of tumor cells. Cancer Res. *63*, 2145–2149.
50. Bearden, S.W., Fetherston, J.D., and Perry, R.D. (1997). Genetic organization of the yersiniabactin biosynthetic region and construction of avirulent mutants in *Yersinia pestis*. Infect. Immun. *65*, 1659–1668.
51. Bobrov, A.G., Kirillina, O., Fosso, M.Y., Fetherston, J.D., Miller, M.C., VanCleave, T.T., Burlison, J.A., Arnold, W.K., Lawrenz, M.B., Garneau-Tsodikova, S., and Perry, R.D. (2017). Zinc transporters YbtX and ZnuABC are required for the virulence of *Yersinia pestis* in bubonic and pneumonic plague in mice. Metallomics *9*, 757–772.
52. Manitz, M.P., Horst, B., Seeliger, S., Strey, A., Skryabin, B.V., Gunzer, M., Frings, W., Schönlau, F., Roth, J., Sorg, C., and Nacken, W. (2003). Loss of S100A9 (MRP14) Results in Reduced Interleukin-8-Induced CD11b Surface Expression, a Polarized Microfilament System, and Diminished Responsiveness to Chemoattractants *In Vitro*. Mol. Cell Biol. *23*, 1034–1043.
53. Shah, S.A., Oakes, R.S., Kapnick, S.M., and Jewell, C.M. (2022). Mapping the Mechanical and Immunological Profiles of Polymeric Microneedles to Enable Vaccine and Immunotherapy Applications. Front. Immunol. *13*, 843355.
54. Dinc, G., Pennington, J.M., Yolcu, E.S., Lawrenz, M.B., and Shirwan, H. (2014). Improving the Th1 cellular efficacy of the lead *Yersinia pestis* rF1-V subunit vaccine using SA-4-1BBL as a novel adjuvant. Vaccine *32*, 5035–5040.
55. Bowen, W., Batra, L., Pulsifer, A.R., Yolcu, E.S., Lawrenz, M.B., and Shirwan, H. (2019). Robust Th1 cellular and humoral responses generated by the *Yersinia pestis* rF1-V subunit vaccine formulated to contain an agonist of the CD137 pathway do not translate into increased protection against pneumonic plague. Vaccine *37*, 5708–5716.
56. Edwards, C., Oakes, R.S., and Jewell, C.M. (2023). Tuning innate immune function using microneedles containing multiple classes of toll-like receptor agonists. Nanoscale *15*, 8662–8674.
57. Sullivan, S.P., Koutsonanos, D.G., Del Pilar Martin, M., Lee, J.W., Zarnitsyn, V., Choi, S.-O., Murthy, N., Compans, R.W., Skountzou, I., and Prausnitz, M.R. (2010). Dissolving polymer microneedle patches for influenza vaccination. Nat. Med. *16*, 915–920.

STAR★METHODS

KEY RESOURCES TABLE

REAGENT or RESOURCE	SOURCE	IDENTIFIER
Antibodies		
Rabbit anti-*Yersinia pestis* serum	This paper.	NA
Alexa Fuor546 Donkey anti-Rabbit IgG381 (H + L)	Invitrogen	A10040; RRID: AB_2534016
Bacterial and virus strains		
Yersinia pestis KIM6+	Bearden et al.[50]	NA
Yersinia pestis znuA ybtX	Bobrov et al.[51]	NA
Yersinia pestis KIM6+ pGEN-luxCDABE	This paper.	NA
Yersinia pestis znuA ybtX pGEN-luxCDABE	This paper.	NA
Yersinia pestis KIM6+ pGEN222-dsRed	This paper.	NA
Experimental models: Organisms/strains		
Mouse: Swiss Webster (CFW)	Charles River	Crl: CFW(SW) Strain Code: 024
Mouse: C57Bl/6J	The Jackson Laboratory	Strain #: 000664
Mouse: C57Bl/6J S100A9−/−	Manitz et al.[52]	NA
Recombinant DNA		
pGEN-luxCDABE	Sun et al.[37]	NA
pGEN222-dsRed	Sun et al.[37]	NA
Other		
Microneedle Arrays	Chandler et al.[29]; Shah et al.[53]	NA

RESOURCE AVAILABILITY

Lead contact

Additional information and requests for resources and reagents used in this study should be directed to and will be fulfilled by the lead contact, Matthew Lawrenz, matt.lawrenz@louisville.edu.

Materials availability

- This study did not generate new unique reagents.
- There are restrictions on the availability of *Y. pestis* strains used in these studies due to Select Agent Regulations.

Data and code availability

- Data reported in this paper will be shared by the lead contact upon request, Matthew Lawrenz, matt.lawrenz@louisville.edu.
- This study does not report any original code.
- Any information related to the data presented in this manuscript can be obtained from the lead contact, Matthew Lawrenz, matt.lawrenz@louisville.edu.

EXPERIMENTAL MODEL AND STUDY PARTICIPANT DETAILS

Animals

C57BL/6J mice were purchased from The Jackson Laboratory and Swiss Webster were purchased from Charles River. S100A9$^{-/-}$ mice[52] were bred at the University of Illinois at Urbana-Champaign prior to transfer to the University of Louisville for infection. Both male and female mice (6–12 weeks in age) were randomly assigned to experimental groups. No sex bias was observed during these studies. Animals were housed in accordance with NIH guidelines and all procedures were approved by the University of Louisville IACUC and the University of Illinois IACUC. Three days prior to challenge with *Y. pestis*, animals were transferred to the University of Louisville's Center for Predictive Medicine Regional Biocontainment Laboratory ABSL-3 facilities to acclimate to the facility. After infection, mice were observed for up to 14 days for the development of moribund disease and humanely euthanized if they met predefined endpoints.

Bacterial strains

Y. pestis KIM6+[50] and *Y. pestis znuA ybtX*[51] were routinely grown in Difco brain heart infusion (BHI) broth (BD Biosciences). Strains transformed with the pGEN-*luxCDABE* or pGEN222-dsRed plasmids[37] were grown in the presence of kanamycin (50 μg/mL). For infection, bacteria were grown overnight at 26°C in BHI broth prior to intradermal challenge. Prior to intranasal instillation, *Y. pestis* was grown overnight at 26°C, diluted to 0.05 OD_{600} in BHI broth with 2.5 mM $CaCl_2$, and grown at 37°C with aeration for 16 to 18 h.[54,55] Bacterial concentrations were determined using a spectrophotometer and diluted to desired concentrations in 1x PBS for intranasal instillation. Concentrations of bacterial inoculums for mouse studies were confirmed by serial dilution and enumeration on agar plates.

METHOD DETAILS

Microneedle array preparation

Microneedle arrays (MNAs) were prepared as previously described.[29,53] Briefly, an MNA containing a total of 77 microneedles in staggered rows (base diameter, 250 μm; spacing between rows, 300 μm; spacing within rows, 1200 μm; height, 650 μm) was replicated using soft lithography. Negative templates were formed using poly(dimethylsiloxane) (Sylgard 184, Dow-Corning). Poly(l-lactide) (PLLA) was then melted through a phase transition in the PDMS molds under vacuum (−25 in. Hg, 200°C, 90 min), then cooled to −20°C for 30 min before separating the cast PLLA MNAs from the PDMS mold. MNAs were then washed in distilled water, followed by 70% ethanol.[56] MNAs were imaged on a using a JEOL 6700F FEG-SEM scanning electron microscope to confirm their morphology (Figure S1A).[53] To characterize the mechanical properties (stiffness and fracture force) of the MNAs, a Dynamic Mechanical Analyzer (DMA) TA Q800 was used in the static force mode using a compression clamp. In brief, the MN array was fixed on the lower plate, and the upper plate was moved toward the MN array with a ramp force of 1 Newton (N) per minute until a force of 8N was reached. The force required to penetrate skin was calculated based on the required force for all 77 projections with this geometry to effectively penetrate skin (Figure S1B).[57] Following preparation, MNAs were sterilized with ethylene oxide before use in subsequent mouse studies.

MNA incubation with *Y. pestis*

To load MNAs with bacteria, MNAs were incubated with *Y. pestis* as previously described.[29] Briefly, *Y. pestis* was diluted to desired concentrations (CFU/mL) in BHI. MNAs were fully submerged in 1 mL of culture in a 24 well-plate and incubated for 30 min with rocking at room temperature. Any bubbles from the culture were gently removed from the MNAs prior to incubation using a pipet tip. Prior to application to the ear, excess medium was removed from the MNAs using a sterile cotton swab.

Animal infections with *Y. pestis*

Mice were challenged with *Y. pestis* as previously described.[37,54,55] For MNA inoculation, mice were anesthetized with isoflurane and the MNA was applied to the left ear. MNA was pressed on the ear for 5 s and then removed with forceps. For intranasal challenge, mice were anesthetized with ketamine/xylazene and administered 20 μL of bacteria suspended in 1X PBS to the left nare. For optical imaging, mice were anesthetized with isoflurane and imaged using the IVIS Spectrum imaging system (Caliper Life Sciences, Hopkinton, MA). Average radiance (photons/sec/cm2) was calculated for ear and lymph nodes as previously described.[37] Infected mice were monitored for the development of disease symptoms twice daily for 14 days. Moribund animals meeting predefined endpoint criteria were humanely euthanized by CO_2 asphyxiation and scored as succumbing to infection 12 h later.

Measurement of bacterial burden in the ear and lymph node

Bacterial numbers in the ear dermal layer and lymph nodes were determined by conventional bacterial enumeration using serial dilutions. Ears were wiped with 70% ethanol prior to remove viable skin-resident bacteria. All tissues were homogenized in sterile PBS using a tissue homogenizer (Omni). 10-fold serial dilutions were made in PBS, and 10 μL were plated in triplicate onto Difco BHI agar (BD Biosciences). Colony forming units (CFU) were counted after incubation at 26°C for 48 h.

IMAGING OF EAR WITH TWO-PHOTON MICROSCOPY

Mouse ears were collected immediately after MNA inoculation *Y. pestis*. Ears, with the MNA attached, were placed into tissue cassettes with sponges to maintain the MNAs within the dermis. Tissues were incubated in 10% formalin for 24 h. Following fixation, tissue cassettes with ears were washed once with 1x PBS and stored in 1x PBS until imaged by two-photon microscopy. For imaging, MNAs were removed and bacteria within the ears were stained by incubation with anti-*Y. pestis* serum (1:1,000) and Alexa Fuor546 Donkey anti-Rabbit IgG (H + L) (1:500; Invitrogen Cat. No. A10040). Tissues were incubated with antibodies overnight in FBS. Mouse ear structures and immune cells were visualized by autofluorescence in the GFP channel.

QUANTIFICATION AND STATISTICAL ANALYSIS

Animal experiments were repeated twice to confirm reproducibility and the data is represented as the combination of the two independent experiments. p values were calculated using Student's *t* test, one-way analysis of variance (ANOVA) with appropriate post hoc testing as indicated in figure legends. Groups size, definition of center, and dispersion and precision measures are also noted in the figure legends as appropriate. All statistics were completed using GraphPad Prism software.